Available online at www.sciencedirect.com
ScienceDirect
Catalysis Today 132 (2008) 101–108
CATALYSIS TODAY
www.elsevier.com/locate/cattod

Catalytic performance and QXAFS analysis of Ni catalysts modified with Pd for oxidative steam reforming of methane

Yuya Mukainakano [a], Kaori Yoshida [a], Kazu Okumura [b], Kimio Kunimori [a], Keiichi Tomishige [a,*]

[a] *Institute of Materials Science, University of Tsukuba, 1-1-1 Tennodai, Tsukuba, Ibaraki 305-8573, Japan*
[b] *Department of Materials Science, Faculty of Engineering, Tottori University, Koyama-cho Minami, Tottori 680-8552, Japan*

Available online 25 January 2008

Abstract

Pd–Ni bimetallic catalysts prepared by co-impregnation and sequential impregnation methods were compared in the catalytic performance in oxidative steam reforming of methane. The sequential impregnation was more effective to the suppression of hot spot formation. According to the structural analysis by *in situ* quick-scanning X-ray absorption fine structure (QXAFS) during the temperature programmed reduction, the sequential impregnation method gave the bimetallic particles with higher Pd surface composition because of the low possibility of the Pd–Ni bond formation. Higher surface composition of Pd with higher reducibility than Ni is connected to the enhancement of the catalyst reducibility and the suppression of the hot spot formation.

Keywords: Oxidative reforming of methane; Steam reforming; Pd; Ni; Thermography; Hot spot; QXAFS; Catalyst reducibility; Surface composition

1. Introduction

Oxidative steam reforming of methane is the combination of the methane steam reforming [Eq. (1)] and dry reforming [Eq. (2)] with catalytic combustion [Eq. (3)] and catalytic partial oxidation of methane [Eq. (4)] [1–6]:

$$CH_4 + H_2O \rightarrow CO + 3H_2 \quad \Delta H^0_{298\,K} = +206\,kJ\,mol^{-1} \qquad (1)$$

$$CH_4 + CO_2 \rightarrow 2CO + 2H_2 \quad \Delta H^0_{298\,K} = +247\,kJ\,mol^{-1} \qquad (2)$$

$$CH_4 + 2O_2 \rightarrow CO_2 + 2H_2O \quad \Delta H^0_{298\,K} = -803\,kJ\,mol^{-1} \qquad (3)$$

$$CH_4 + \frac{1}{2}O_2 \rightarrow CO + 2H_2 \quad \Delta H^0_{298\,K} = -36\,kJ\,mol^{-1} \qquad (4)$$

It has been known that oxidative steam reforming of methane can be more energy efficient than the conventional methane steam reforming. This is because conventional steam reforming requires an external heat supply and, in contrast, oxidative steam reforming of methane can be an internal heating process. Therefore, the oxidative steam reforming of methane is one of the promising methods for the production of synthesis gas from natural gas. However, it has been reported that hot spot formation is a problem in the oxidative steam reforming of methane [7–9] and this is also a common problem in the reforming of hydrocarbons using oxygen. It is known that metallic nickel is an active component for the reforming reaction. However, in the presence of oxygen, the Ni species can be easily oxidized and can thereby lose their reforming activity [3,10,11]. On the other hand, the oxidized Ni species can catalyze methane combustion reaction, and this can increase the catalyst bed temperature drastically to give a hot spot. Our group has reported that the modification of Ni catalysts with small amount of noble metals such as Pt and Pd is effective to the suppression of hot spot formation in the oxidative steam reforming of methane [11–14]. This modification effect is caused by the formation of noble metals-Ni bimetallic particles and the enhancement of catalyst reducibility promoted by the presence of noble metals. The suppression of hot spot formation is explainable by the overlap of the combustion reaction zone with the reforming reaction zone on the catalysts with high reducibility. Another important point is that this property is strongly influenced by the

* Corresponding author. Tel.: +81 29 853 5030; fax: +81 29 853 5030.
E-mail address: tomi@tulip.sannet.ne.jp (K. Tomishige).

0920-5861/$ – see front matter © 2007 Elsevier B.V. All rights reserved.
doi:10.1016/j.cattod.2007.12.031

preparation method of bimetallic catalysts. This is because the different preparation method can give the bimetallic particles with different microstructures. We have reported that the sequential impregnation method is more suitable than the conventional co-impregnation method [9,11,14], and this is related to the surface segregation of noble metal atoms on the bimetallic particles. In this article, our purpose is to pursue the formation mechanism of Pd–Ni bimetallic particles during the preparation in two different methods by means of quick-scanning X-ray absorption fine structure.

2. Experimental

2.1. Catalyst preparation

A commercially available γ-Al_2O_3 (JRC-ALO-1) (Catalysis Society of Japan, S_{BET} = 143 $m^2\,g^{-1}$, grain size of 2–3 mm) was calcined at 1123 K in air for 3 h; it was used as a support material. The support thus obtained had a specific surface area of 110 $m^2\,g^{-1}$. It was crushed and sieved to particle sizes between 180 and 250 μm before impregnation. Supported monometallic Ni and Pd catalysts were prepared respectively using the impregnation method with the aqueous solutions of $Ni(NO_3)_2{\cdot}6H_2O$ (99.9%, Wako Pure Chemical Industries Ltd.) and $PdCl_2$ (99.9%, Soekawa Chemical Co. Ltd.). After removal of the solvent by heating and evaporation at 353 K, the resulting products were dried in an oven at 383 K for 12 h. Subsequently, the samples were calcined at 773 K in air for 3 h. Bimetallic catalysts (Pd–Ni) were prepared using two methods. One is the sequential (two-step) impregnation method. The calcined monometallic nickel catalyst was reduced at 1123 K for 0.5 h under H_2 flow, and then this treated sample was impregnated with an acetone solution of $Pd(C_5H_7O_2)_2$ (99.9%; Soekawa Chemical Co. Ltd.) under air atmosphere. After removal of the acetone solvent, the catalyst was dried at 383 K for 12 h and calcined in air at 573 K for 3 h. The resultant catalyst is denoted as Pd/Ni. The other method is co-impregnation. The precursor is a mixed aqueous solution of $Ni(NO_3)_2{\cdot}6H_2O$ and $PdCl_2$. After co-impregnation, the preparation procedure is identical to that of the monometallic catalysts. This resultant catalyst is denoted as Pd + Ni. The number in parentheses refers to the weight percent of the catalyst's metallic component. On the Pd(0.1)/Ni(0.9) and Pd(0.1) + Ni(0.9) catalysts, the molar ratio of Pd to Ni is 1/17.

2.2. Activity test and thermographical observation

Oxidative steam reforming of methane was conducted under atmospheric pressure in a fixed-bed quartz reactor (i.d. 4 mm Ø, o.d. 6 mm Ø). A schematic diagram of the reactor and pictures of catalyst granules in the quartz reactor are illustrated in Fig. 1, along with one exemplary thermographical image. The quartz reactor had an axial thermowell (o.d. 1.5 mm Ø) containing a chromel–alumel thermocouple located at the outlet of the catalyst bed, which was used for temperature control. An electric furnace was connected with this thermo-controller; it had a window (15 mm × 15 mm) for observation of the temperature profile of catalyst granules. The temperature profile was measured using infrared thermograph equipment (TH31; NEC San-ei Instruments Ltd.). Fig. 1 shows that the radial temperature gradient was rather flat in the A cross-section, indicating that the gas flow is close to a plug flow condition. Therefore, we show only the temperature profile along the B cross-section in Section 3. The catalyst (0.08 g) was reduced in the hydrogen flow (30 ml min^{-1}, 100% H_2) at 1123 K for 0.5 h in the reactor. After reduction, the feed gases (the mixture of CH_4, O_2, steam and Ar) were introduced to the catalyst bed at various contact times W/F (W(g) = catalyst weight, F(mol h^{-1}) = total flow rate of gases). Gases such as CH_4, O_2, H_2 and Ar used here were research grade; they were obtained from Takachiho Trading Co. Ltd. The gases were used without further purification. Steam was obtained by vaporizing distilled water and the water was supplied continuously using a feeding pump (MT2111, Moleh Ltd.). The partial pressure ratio of the feeding gases is $CH_4/H_2O/O_2/Ar$ = 40/30/20/10. An iced water trap was located at the reactor exit to remove the steam contained in the effluent gas. The gas was collected from the sampling port using a micro-syringe. Then it was analyzed using a gas chromatograph (GC-14A; Shimadzu Corp.) equipped with a flame ionization detector (FID) and a thermal conductivity detector (TCD). Concentrations of CO, CO_2 and CH_4 in the effluent gas were determined using an FID-GC equipped with a methanator and a stainless steel column packed with Gaskuropack 54 (GL Science). The H_2 concentration was determined using TCD-GC with a stainless steel column packed with a molecular sieve 13×. Methane conversion and CO selectivity in oxidative steam reforming of methane were calculated as described below:

$$\text{methane conversion}\,(\%) = \frac{C_{CO}+C_{CO_2}}{C_{CH_4}+C_{CO}+C_{CO_2}} \times 100$$

$$\text{CO selectivity}\,(\%) = \frac{C_{CO}}{C_{CO}+C_{CO_2}} \times 100$$

C, concentration of each gas in the effluent gas.

The amount of deposited coke during the reaction was able to be neglected in all the cases presented here, although the coke deposition has often been observed in methane reforming [15–18]. The catalytic performance in steam reforming of methane was also evaluated. The method and procedure were the same as those oxidative steam reforming of methane except for the partial pressure ratio ($CH_4/H_2O/Ar$ = 30/30/40) and reaction temperature (1073 K).

2.3. Catalyst characterization

Temperature programmed reduction (TPR) profiles were measured in a fixed bed quartz reactor. In each experiment, 0.01 g of sample was loaded into the quartz reactor and heated with a heating rate of 10 K min^{-1}, from room temperature to 1123 K in 5% hydrogen diluted in Ar (30 ml min^{-1}) as a reducing gas. Water produced during the reduction was removed using a cold trap with frozen acetone (ca. 173 K). The TPR profile was monitored continuously with an on-line TCD-GC. The H_2 consumption was estimated from the

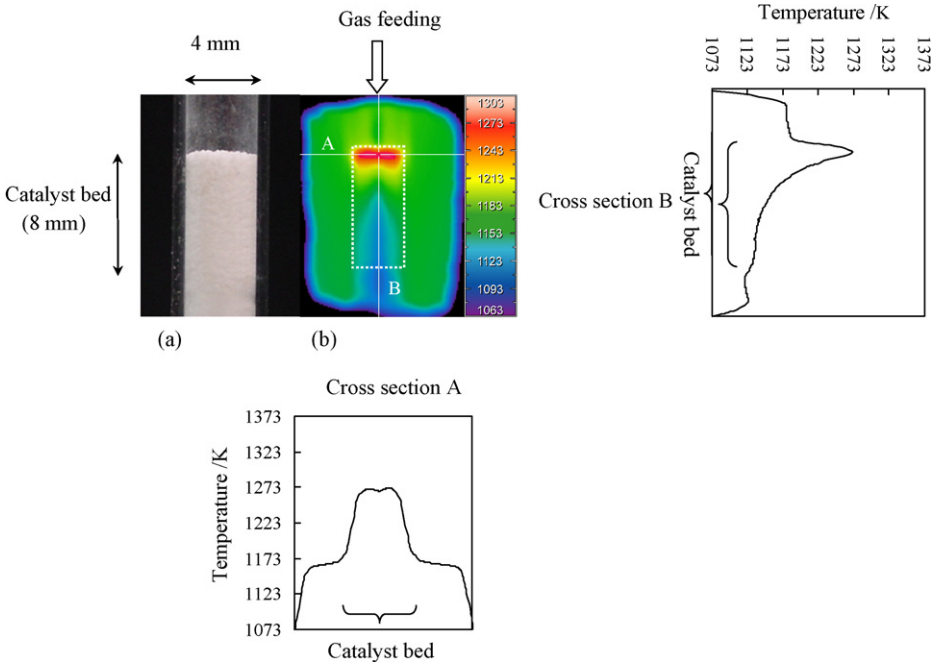

Fig. 1. Picture of catalyst granules in the quartz glass tube (a) before reaction at room temperature and (b) one example of thermographical image during the oxidative steam reforming of methane.

integrated peak area of the reduction profiles.The Pd *K*-edge quick-scanning X-ray absorption fine structure (QXAFS) was measured at the BL01B1 station in the SPring-8 with the approval of the Japan Synchrotron Radiation Research Institute (JASRI) (Proposal No. 2006A1058). The storage ring was operated at 8 GeV. A Si(1 1 1) single crystal was used to obtain a monochromatic X-ray beam. Two ion chambers filled with 50% Ar + 50% N_2 and 75% Ar + 25% Kr were used as detectors of I_0 and I, respectively. The samples for the XAFS measurement were prepared by pressing about 1 g catalyst powder, and the thickness of Pd *K*-edge XAFS was 12 mm to give 0.14 edge jump. The samples were transferred to the measurement cell. The sample was heated with a ramping rate of 5 K min^{-1} in 5% H_2 diluted in Ar (30 ml min^{-1}) under atmospheric pressure. The experiment was carried out in a similar manner to the previously reported method [19]. The Si(1 1 1) single crystal was moved to obtain an X-ray beam with continuous energy. The Si(1 1 1) monochromator was continuously moved from 4.8° to 4.4° in 1 min. XAFS data were collected in a transmission mode under *in situ* conditions. For XAFS analysis, the oscillation was first extracted from the XAFS data by a spline smoothing method [20]. The oscillation was normalized by the edge height around 50 eV. The Fourier transformation of the k^3-weighted EXAFS oscillation from k space to r space was performed to obtain a radial distribution function. The inversely Fourier filtered data were analyzed by a usual curve fitting method [21,22]. For the curve fitting analysis, the empirical phase shift and amplitude functions for Pd–O and Pd–Pd were extracted from the data for PdO and Pd foil, respectively, that were measured at the same temperature for the analysis of samples. Theoretical functions for the Pd–Ni bond were calculated using the FEFE8.2 program [23]. The analysis of EXAFS data was performed using the ''REX2000'' program (RIGAKU Co., Version: 2.3.3).

3. Results and discussion

3.1. Catalytic performance and catalysts bed temperature profile in oxidative steam reforming of methane

The catalytic performance in terms of the methane conversion, H_2/CO ratio and CO selectivity over Ni(0.9), Pd(0.1), Pd(0.1) + Ni(0.9) and Pd(0.1)/Ni(0.9) are listed in Table 1 and the temperature profiles obtained from thermo-

Table 1
Catalytic performance in oxidative steam reforming of methane

Catalyst	*W*/*F* (g (h/mol))	CH_4 conversion (%)	H_2/CO	CO selectivity (%)
Ni(0.9)	0.12	76	2.5	75
Ni(2.6)	0.12	>99	2.8	80
Pd(0.1)	0.12	56	1.4	89
Pd(0.1) + Ni(0.9)	0.12	>99	2.8	80
Pd(0.1)/Ni(0.9)	0.12	>99	2.8	81
Equilibrium	–	>99	2.9	81

Reaction conditions: $CH_4/H_2O/O_2/Ar = 40/30/20/10$; temperature 1123 K; total pressure 0.1 MPa; catalyst weight 0.08 g; H_2 pretreatment at 1123 K.

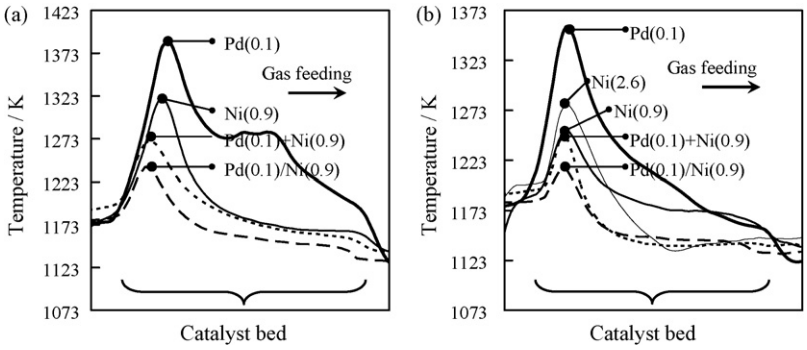

Fig. 2. Temperature profiles of the catalyst bed in oxidative steam reforming of methane over various catalysts at *W/F* (g (h/mol)) = 0.07 (a) and 0.12 (b). Reaction conditions: $CH_4/H_2O/O_2/Ar$ = 40/30/20/10; temperature 1123 K; total pressure 0.1 MPa; catalyst weight 0.08 g; H_2 pretreatment at 1123 K.

graphical observation are shown in Fig. 2. The order of the methane conversion at the *W/F* = 0.12 g (h/mol) was as follows: Pd(0.1)/Ni(0.9) ≈ Pd(0.1) + Ni(0.9) > Ni(0.9) > Pd (0.1). In particular, methane conversion on both Pd–Ni catalysts was as high as that at the reaction equilibrium. Therefore, it is impossible to compare the catalytic activity between Pd(0.1)/Ni(0.9) and Pd(0.1) + Ni(0.9). However, it became possible under severer reaction conditions such as lower temperature and lower *W/F*. In fact, at *W/F* = 0.07 g (h/mol) and reaction temperature of 1073 K, the methane conversion on Pd(0.1)/Ni(0.9) and Pd(0.1) + Ni(0.9) were 96.5 and 93.0%, respectively. As a result, Pd(0.1)/Ni(0.9) showed higher activity than Pd(0.1) + Ni(0.9). As a reference, we evaluated the catalytic performance in methane steam reforming over Ni(0.9), Pd(0.1) + Ni(0.9) and Pd(0.1)/Ni(0.9) as listed in Table 2. The order of methane conversion was as follows: Ni(0.9) > Pd(0.1) + Ni(0.9) > Pd(0.1)/Ni(0.9). From the comparison between methane steam reforming with and without oxygen, it is found that the Ni(0.9) catalyst had high activity of methane steam reforming, however, the catalyst is not suitable to oxidative steam reforming of methane. This indicates that the addition of oxygen to the reactant gas drastically decreased the performance in oxidative reforming. This behavior corresponds to the deactivation due to the oxidation of Ni metal active for the reforming reactions. In contrast, the Pd(0.1)/Ni(0.9) catalyst was not so active as Ni(0.9) in methane steam reforming, however, high conversion was given by Pd(0.1)/Ni(0.9) in oxidative steam reforming of methane. Based on the low performance of Pd(0.1) in both methane reforming, the synergy between Pd and Ni can enhance the performance of Pd–Ni bimetallic catalysts, in particular, Pd(0.1)/Ni(0.9), in oxidative steam reforming of methane.

Fig. 2 shows the thermographical observation during oxidative steam reforming of methane at *W/F* = 0.07 and 0.12 g (h/mol) over Ni(0.9), Pd(0.1), Pd(0.1) + Ni(0.9) and Pd(0.1)/Ni(0.9). On all the catalysts, the exothermic profile near the catalyst bed inlet was observed, although the maximum temperature was dependent on the catalysts. Under both *W/F* conditions, the Pd(0.1) catalyst exhibited very high catalyst bed temperature. This is related to low methane conversion on Pd(0.1). Under the partial pressure conditions of $CH_4/H_2O/O_2/Ar$ = 40/30/20/10, 25% methane conversion is contributed to methane combustion, and methane conversion beyond 25% is assigned to methane reforming reactions. Since oxygen conversion was almost 100% in all the experimental results shown here, low methane conversion means small contribution of methane reforming reactions. As listed in Table 1, methane conversion of Pd(0.1) was smaller than other catalysts, and smaller reforming contribution causes higher temperature profile. The tendency of Ni(0.9) and Ni(2.6) catalysts as shown in Fig. 2(b) is different from the case of Pd(0.1) because the Ni(2.6) gave high methane conversion (Table 1). On the basis that the Ni species is oxidized near the catalyst bed inlet, where the combustion reaction proceeds mainly, the highest bed temperature is influenced by the combustion activity of the Ni catalysts, which is higher on larger Ni loading amount. Furthermore, the bed temperature on the Ni catalysts decreased steeply in the catalyst bed. This corresponds to the endothermic profile of the reforming reactions. In the downstream part after oxygen is completely consumed, the metallic Ni can be maintained and it is very active for the reforming reactions. This means that the exothermic combustion reaction zone and endothermic reforming reaction zone are separated in the catalyst bed, and this phenomenon is connected to the large gradient in the bed temperature. In contrast, the temperature

Table 2
Catalytic performance in steam reforming of methane

Catalyst	*W/F* (g (h/mol))	CH_4 conversion (%)	H_2/CO	CO selectivity (%)
Ni(0.9)	0.40	76	3.3	89
Pd(0.1) + Ni(0.9)	0.40	73	3.4	85
Pd(0.1)/Ni(0.9)	0.40	57	3.5	80
Equilibrium	–	87	3.1	96

Reaction conditions: $CH_4/H_2O/Ar$ = 30/30/40; temperature 1073 K; total pressure 0.1 MPa; catalyst weight 0.08 g; H_2 pretreatment at 1123 K.

gradient of Pd–Ni bimetallic catalysts was much smaller than that of Pd(0.1), Ni(0.9) and Ni(2.6). The effect was more remarkable on Pd(0.1)/Ni(0.9) than Pd(0.1) + Ni(0.9). This can be explained by the overlap between the combustion reaction zone and the reforming reaction zone because of the enhancement of reducibility of Ni species promoted by the Pd addition. It is interpreted that the promoting effect of Pd introduced by the sequential impregnation is more remarkable than that by the co-impregnation. This result suggests that the interaction between Pd and Ni is strongly influenced by the preparation methods. Therefore, the microstructure of Pd–Ni bimetallic catalysts was analyzed by means of XAFS. In particular, we focused on the structural change during the reduction pretreatment since the interaction between Pd and Ni is formed using *in situ* Pd K-edge QXAFS.

3.2. Characterization during the reduction pretreatment by means of TPR and QXAFS

Before measuring the *in situ* QXAFS, temperature-programmed reduction (TPR) profiles were obtained to evaluate the catalyst reducibility. Fig. 3 shows TPR profiles of various catalysts. The H_2 consumption profile of Ni(0.9) were observed in the temperature range of 700–1160 K as shown in Fig. 3(a). The ratio of total hydrogen consumption to Ni content was almost 100%. This H_2 consumption peak is assigned to the reduction of highly dispersed Ni^{2+} species interacted strongly with the Al_2O_3 surface [11,13,24]. In the case of Pd(0.1) + Ni(0.9) (Fig. 3(b)), a small consumption peak at 433 K is assigned to the reduction of Pd, and the main reduction peak started at about 563 K, which is about 200 K lower than the case of Ni(0.9). This is the promoting effect of Pd on the reduction of Ni species. On the other hand, Pd(0.1)/Ni(0.9) showed a sharp peak at about 563 K (Fig. 3(c)), which is assigned to the reduction of NiO interacted weakly with Al_2O_3 [11,13,25,26]. This NiO is originated from Ni metal particles formed during the H_2 reduction before the second impregnation in the preparation by sequential impregnation. According to our previous report, the reduction of the NiO species without noble metal addition was observed at 600 K in the TPR profile [14]. The reduction peak was shifted to 40 K lower temperature by the addition of Pd. A part of Ni species on Pd(0.1)/Ni(0.9) is reduced at almost the same temperature as that on Pd(0.1) + Ni(0.9). From the comparison of the TPR profiles between Pd(0.1)/Ni(0.9) and Pd(0.1) + Ni(0.9), it is found that the state of Ni species is strongly dependent on the preparation method. From the comparison between catalytic performance and TPR results, the Pd–Ni bimetallic catalyst with higher catalyst reducibility tends to have higher catalytic performance in the oxidative steam reforming of methane.

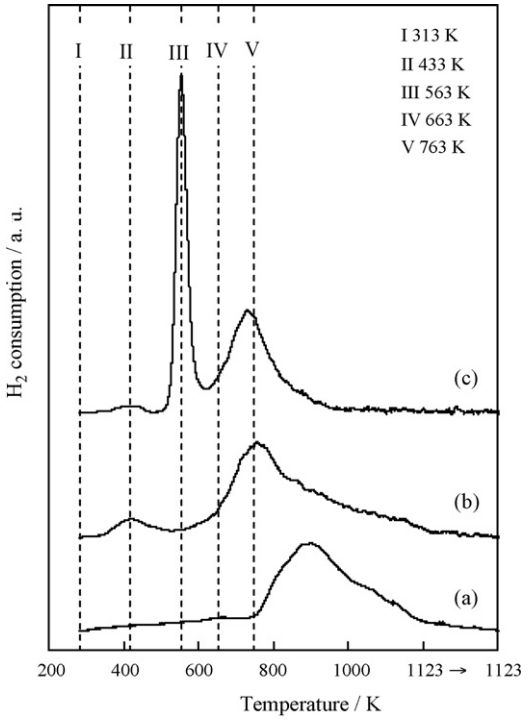

Fig. 3. Temperature-programmed reduction profiles of fresh catalysts. (a) Ni(0.9), (b) Pd(0.1) + Ni(0.9), and (c) Pd(0.1)/Ni(0.9). I–V correspond to the temperatures where *in situ* QXAFS data are shown in Figs. 4 and 5, and Tables 3 and 4.

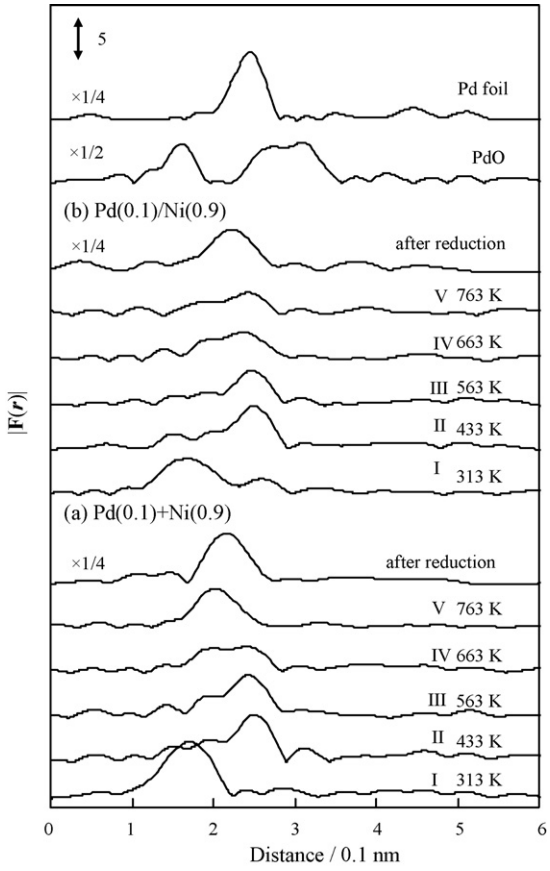

Fig. 4. Results of Fourier transform of Pd *K*-edge XAFS oscillation of (a) Pd(0.1) + Ni(0.9) and (b) Pd(0.1)/Ni(0.9) during the H_2 reduction and after H_2 reduction. The results of Ni foil, Pd foil, and PdO are also shown as a reference. FT range: 30–120 nm^{-1}. Temperature ramping rate; 5 K/min. Pretreatment conditions are the same as those in Tables 3 and 4. The data on the samples after reduction were measured at room temperature.

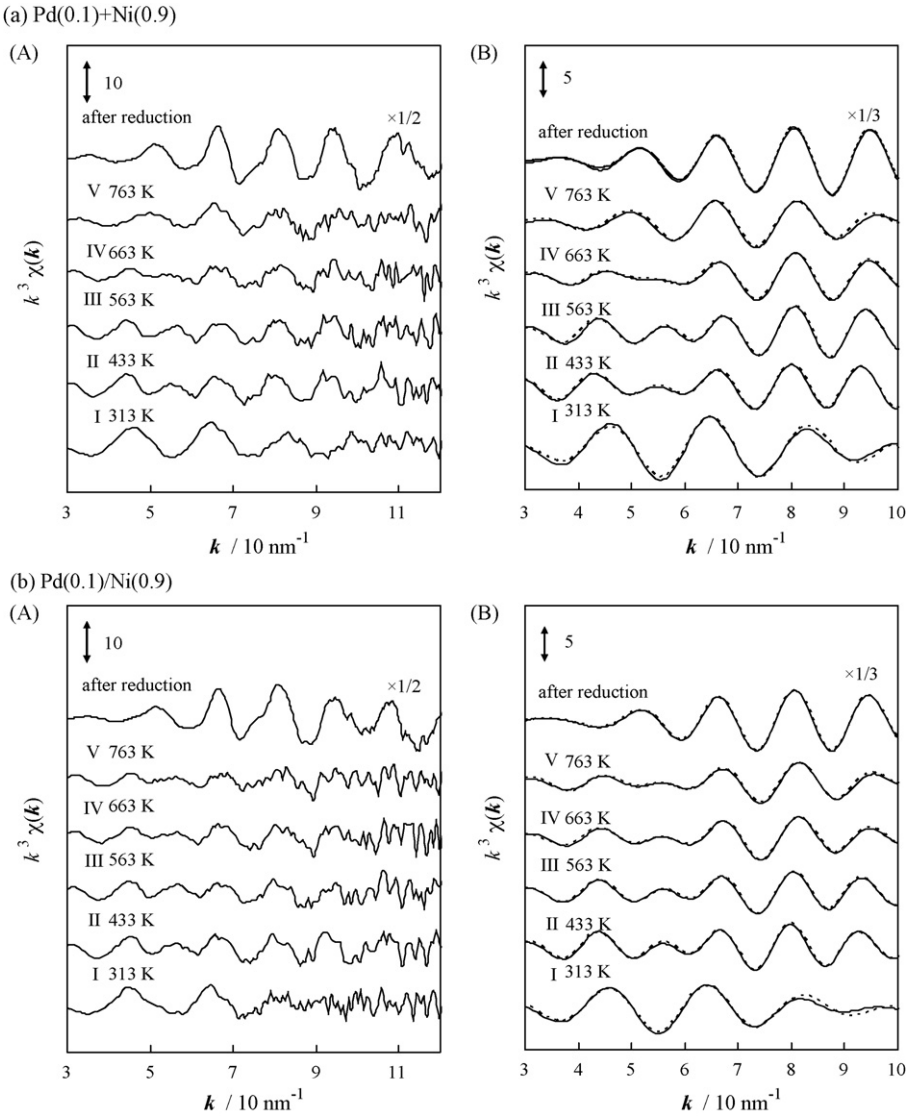

Fig. 5. Results of Pd *K*-edge XAFS analysis of Pd(0.1) + Ni(0.9) (a) and Pd(0.1)/Ni(0.9) (b) catalysts: (A) k^3-weighted oscillations; (B) Fourier filtered data (solid line) and calculated data (dotted line) based on the curve fitting results listed in Tables 3 and 4. FT range: 30–120 nm^{-1}. The data on the samples after reduction were measured at room temperature.

Fig. 4 shows the Fourier transforms of Pd *K*-edge XAFS of Pd(0.1) + Ni(0.9) and Pd(0.1)/Ni(0.9) during H_2 reduction, and Fig. 5 shows the k^3-weighted Pd *K*-edge XAFS oscillations. Curve fitting results are summarized in Tables 3 and 4. On both Pd(0.1) + Ni(0.9) and Pd(0.1)/Ni(0.9) catalysts, the XAFS spectra at 313 K were fitted by the Pd–O bond. The fitting was not so good, and this is probably because there are some kinds of the Pd–O bonds with similar bond length such as oxide ions on the support surface, hydroxide species or small PdO cluster. In the case of Pd(0.1) + Ni(0.9) at 433 and 563 K, the Pd–Pd bond appeared and the coordination number of Pd–O was lower than that at 313 K. This represents that the Pd species is reduced to form small Pd metal cluster. This similar structural change was also observed on Pd(0.1)/Ni(0.9) at 433 and 563 K. One of the important points on Pd(0.1)/Ni(0.9) is that the Pd–Ni bond was not observed at all (Table 4), although the reduction profile of Ni species was clearly observed at 563 K (Fig. 3(c)). The behavior of the Pd–Ni bond formation over Pd(0.1) + Ni(0.9) is different. In the case of Pd(0.1) + Ni(0.9) at 663 K, the Pd–Ni bond formation was observed and this agreed well with the TPR profile, and the tendency was more significant at 763 K. On the other hand, the contribution of the Pd–Ni bond on Pd(0.1)/Ni(0.9) was much smaller than that on Pd(0.1) + Ni(0.9) at both 663 and 763 K. The results of *in situ* QXAFS on both catalysts indicate that the temperature of the Pt–Ni bond formation is influenced by preparation methods. These behaviors are maintained on the catalysts after the reduction pretreatment. The data of the Pd(0.1) + Ni(0.9) and Pd(0.1)/Ni(0.9) catalysts after reduction are also shown in Figs. 4 and 5, and they are also listed in Tables 3 and 4. These spectra were obtained at room temperature. In the case of Pd(0.1) + Ni(0.9), only the Pd–Ni bond was observed, however, the Pd–Pd bond disappeared. This is also extended by the decrease of the coordination number of the Pd–Pd bond with increasing the temperature in *in situ*

Table 3
Curve fitting results of *in situ* Pd *K*-edge QXAFS of Pd(0.1) + Ni(0.9) during TPR and XAFS after reduction

Temperature (K)	Shells	*CN*[a]	*R* ($\times 10^{-1}$ nm)[b]	σ ($\times 10^{-1}$ nm)[c]	ΔE_0 (eV)[d]	R_f (%)[e]
313 (I)	Pd–O	6.6	2.09	0.089	13.5	1.8
433 (II)	Pd–Pd	6.4	2.75	0.089	3.0	0.8
	Pd–O	1.5	2.07	0.095	6.8	
563 (III)	Pd–Pd	5.9	2.72	0.095	2.0	1.1
	Pd–O	0.7	2.14	0.082	11.6	
663 (IV)	Pd–Pd	4.8	2.69	0.111	−0.3	1.0
	Pd–Ni	1.5	2.51	0.096	−9.2	
763 (V)	Pd–Pd	3.5	2.68	0.120	−1.7	1.5
	Pd–Ni	2.4	2.48	0.101	−9.4	
After reduction[f]	Pd–Ni	7.1	2.54	0.069	1.7	1.0

FT range: 30–120 nm^{-1}, Fourier filtering range: 0.170–0.282 nm. I–V correspond to the temperatures in Fig. 2.
[a] Coordination number.
[b] Bond distance.
[c] Debye-Waller factor.
[d] Difference in the origin of photoelectron energy between the reference and the sample.
[e] Residual factor.
[f] The data on the samples after reduction were measured at room temperature.

QXAFS data. The Pd–Ni bond length (0.254 nm) was close to that of the Ni–Ni bond (0.249 nm) and it was much shorter than that of the Pd–Pd bond (0.272 nm). This indicates that Pd atoms can be solved to Ni metal and to form Pd–Ni alloy [27–29]. As a result, it is found that the co-impregnation method gave the well mixture of Pd and Ni. On the other hand, in the case of Pd(0.1)/Ni(0.9) after the reduction, both Pd–Pd and Pd–Ni bonds were observed. When Pd(0.1)/Ni(0.9) was reduced at 1123 K, the interaction between Pd and Ni was formed. However, the degree of mixture between Pd and Ni on Pd(0.1)/Ni(0.9) is not so high as that on Pd(0.1) + Ni(0.9). This can be related to the small contribution of the Pd–Ni bond even at 763 K as listed in Table 4. Lower degree of mixture is due to larger size of NiO particles on Pd(0.1)/Ni(0.9) before the reduction pretreatment as observed in Fig. 3(c). It is suggested that the presence of Pd promoted the reduction of NiO particles to Ni metal particles, for example, via spillover hydrogen from Pd metal clusters [30,31]. The Pd species is interacted with Ni after Ni metal particles are formed, therefore, the possibility of the presence of Pd atoms on the surface of particles is expected to be higher on Pd(0.1)/Ni(0.9) than Pd(0.1) + Ni(0.9), on which Pd species is interacted with highly dispersed Ni species at lower tempera-

Table 4
Curve fitting results of *in situ* Pd *K*-edge QXAFS of Pd(0.1)/Ni(0.9) during TPR and XAFS after reduction

Temperature (K)	Shells	*CN*[a]	*R* ($\times 10^{-1}$ nm)[b]	σ ($\times 10^{-1}$ nm)[c]	ΔE_0 (eV)[d]	R_f (%)[e]
313 (I)	Pd–O	7.5	2.11	0.116	14.3	2.6
433 (II)	Pd–Pd	6.8	2.76	0.105	4.2	1.0
	Pd–O	1.4	2.11	0.083	11.3	
563 (III)	Pd–Pd	4.9	2.75	0.096	4.5	0.9
	Pd–O	1.0	2.07	0.087	9.0	
663 (IV)	Pd–Pd	4.9	2.71	0.110	2.1	
	Pd–O	0.8	2.03	0.080	−0.8	0.6
	Pd–Ni	0.7	2.49	0.227	−4.9	
763 (V)	Pd–Pd	5.3	2.69	0.112	1.3	1.4
	Pd–Ni	1.2	2.51	0.109	−6.8	
After reduction[f]	Pd–Pd	2.5	2.73	0.072	5.9	1.0
	Pd–Ni	5.4	2.53	0.073	1.3	

FT range: 30–120 nm^{-1}, Fourier filtering range: 0.170–0.282 nm. I–V correspond to the temperatures in Fig. 2.
[a] Coordination number.
[b] Bond distance.
[c] Debye-Waller factor.
[d] Difference in the origin of photoelectron energy between the reference and the sample.
[e] Residual factor.
[f] The data on the samples after reduction were measured at room temperature.

ture and these Pd–Ni mixtures are aggregated to form larger particles. Based on the results of XAFS analysis, the surface composition of Pd species is enhanced by the sequential impregnation method. Similar tendency has been also observed in the previous reports [11,14]. This is supported by the activity order in steam reforming of methane (Ni(0.9) > Pd(0.1) + - Ni(0.9) > Pd(0.1)/Ni(0.9)). The Pd species has very low activity in the reforming reactions, and higher surface composition of Pd is connected to lower catalytic activity of steam reforming. On the other hand, in the case of oxidative steam reforming, hot spot formation and large temperature gradient is suppressed by the overlap of the exothermic and endothermic reactions and this is brought by the inhibition of oxidation of Ni. Higher surface composition of Pd with higher reducibility than Ni can enhance the catalyst reducibility.

4. Conclusions

(1) As a result of the catalyst bed temperature profile during the oxidative steam reforming of methane, the temperature gradient over the Pd/Ni bimetallic catalyst prepared by the sequential impregnation method was much smaller than that over the Pd + Ni catalyst prepared by the co-impregnation method and monometallic Ni catalyst. This property can be related to the suppression of hot spot formation.

(2) *In situ* Pd K-edge QXAFS analysis of the Pd–Ni catalysts during the temperature programmed reduction with H_2 revealed the formation process and structural difference of the Pd–Ni bimetallic particles. In the case of the Pd + Ni catalyst, the interaction between Pd and Ni was observed at lower reduction temperature, and as a result, the bimetallic particles with a well mixture of Pd and Ni are formed. In contrast, in the case of the Pd/Ni catalyst, the interaction between Pd and Ni was so small at 763 K, and it is suggested that the bimetallic particles with the surface segregation of Pd atoms are formed. Therefore, the preparation method can influence the surface composition and the sequential impregnation enhanced the surface composition of Pd. This is connected to the flat temperature in oxidative steam reforming of methane by the enhancement of the catalyst reducibility on the Pd/Ni catalyst.

Acknowledgments

This study is supported by the Industrial Technology Research Grant Program (05A43002C) of the New Energy and Industrial Technology Development Organization (NEDO) of Japan.

References

[1] K. Takehira, T. Shishido, P. Wang, T. Kosaka, K. Takaki, J. Catal. 221 (2004) 43.
[2] V.R. Choudhary, K.C. Mondal, A.S. Mamman, J. Catal. 233 (2005) 36.
[3] K. Nagaoka, A. Jentys, J.A. Lercher, J. Catal. 229 (2005) 185.
[4] K. Tomishige, S. Kanazawa, K. Suzuki, M. Asadullah, M. Sato, K. Ikushima, K. Kunimori, Appl. Catal. A: Gen. 233 (2002) 35.
[5] B. Li, K. Maruyama, M. Nurunnabi, K. Kunimori, K. Tomishige, Appl. Catal. A: Gen. 275 (2004) 157.
[6] M. Nurunnabi, Y. Mukainakano, S. Kado, T. Miyao, S. Naito, K. Okumura, K. Kunimori, K. Tomishige, Appl. Catal. A: Gen. 325 (2007) 154.
[7] B. Li, K. Maruyama, M. Nurunnabi, K. Kunimori, K. Tomishige, Ind. Eng. Chem. Res. 44 (2005) 485.
[8] B. Li, R. Watanabe, K. Maruyama, K. Kunimori, K. Tomishige, Catal. Today 104 (2005) 7.
[9] B. Li, R. Watanabe, K. Maruyama, M. Nurunnabi, K. Kunimori, K. Tomishige, Appl. Catal. A: Gen. 290 (2005) 36.
[10] M. Nurunnabi, Y. Mukainakano, S. Kado, B. Li, K. Kunimori, K. Suzuki, K. Fujimoto, K. Tomishige, Appl. Catal. A: Gen. 299 (2006) 145.
[11] B. Li, S. Kado, Y. Mukainakano, T. Miyazawa, T. Miyao, S. Naito, K. Okumura, K. Kunimori, K. Tomishige, J. Catal. 245 (2007) 144.
[12] K. Tomishige, S. Kanazawa, S. Ito, K. Kunimori, Appl. Catal. A: Gen. 244 (2003) 71.
[13] B. Li, S. Kado, Y. Mukainakano, M. Nurunnabi, T. Miyao, S. Naito, K. Kunimori, K. Tomishige, Appl. Catal. A: Gen. 304 (2006) 62.
[14] Y. Mukainakano, B. Li, S. Kado, T. Miyazawa, K. Okumura, T. Miyao, S. Naito, K. Kunimori, K. Tomishige, Appl. Catal. A: Gen. 318 (2007) 252.
[15] K. Tomishige, Y. Himeno, Y. Matsuo, Y. Yoshinaga, K. Fujimoto, Ind. Eng. Chem. Res. 39 (2000) 1891.
[16] K. Tomishige, Y. Chen, K. Fujimoto, J. Catal. 181 (1999) 91.
[17] O. Yamazaki, K. Tomishige, K. Fujimoto, Appl. Catal. A: Gen. 136 (1996) 49.
[18] M. Nurunnabi, S. Kado, K. Suzuki, K. Fujimoto, K. Tomishige, K. Kunimori, Catal. Commun. 7 (2006) 488.
[19] K. Okumura, K. Yoshino, K. Kato, M. Niwa, J. Phys. Chem. B 109 (2005) 12380.
[20] J.W. Cook, D.E. Sayers, J. Appl. Phys. 52 (1981) 5024.
[21] K. Okumura, J. Amano, N. Yasunobu, M. Niwa, J. Phys. Chem. B 104 (2000) 1050.
[22] K. Okumura, S. Matsumoto, N. Nishiaki, M. Niwa, Appl. Catal. B: Environ. 40 (2003) 151.
[23] A.L. Ankudinov, B. Ravel, J.J. Rehr, S.D. Conradson, Phys. Rev. B 58 (1998) 7565.
[24] J. Wang, L. Dong, Y.-H. Hu, G.-S. Zheng, Z. Hu, Y. Chen, J. Solid State Chem. 157 (2001) 274.
[25] Y.-J. Chu, Z.-B. Wei, S.-W. Yang, C. Li, Q. Xin, E.-Z. Min, Appl. Catal. A: Gen. 176 (1999) 17.
[26] S.-B. Wang, G.-Q. Lu, Appl. Catal. A: Gen. 169 (1998) 271.
[27] M. Nurunnabi, Y. Mukainakano, S. Kado, T. Miyazawa, K. Okumura, T. Miyao, S. Naito, K. Suzuki, K. Fujimoto, K. Kunimori, K. Tomishige, Appl. Catal. A: Gen. 308 (2006) 1.
[28] S. Takenaka, Y. Shigeta, E. Tanabe, K. Otsuka, J. Phys. Chem. B. 108 (2004) 7656.
[29] C. Crisafulli, S. Scirè, R. Maggiore, S. Minicò, S. Galvagno, Catal. Lett. 59 (1999) 21.
[30] R. Ueda, T. Kusakari, K. Tomishige, K. Fujimoto, J. Catal. 194 (2000) 14.
[31] K. Tomishige, A. Okabe, K. Fujimoto, Appl. Catal. A: Gen. 194–195 (2000) 383.